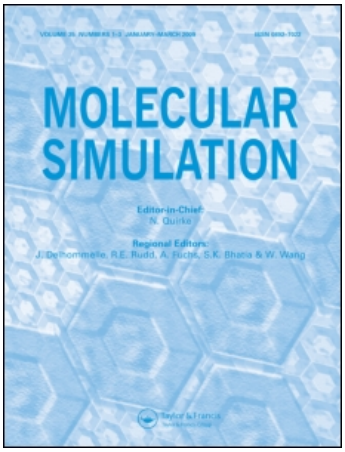

Molecular Simulation
Publication details, including instructions for authors and subscription information:
http://www.informaworld.com/smpp/title~content=t713644482

ALLD: An object-oriented mesoscopic simulation program for polar biomolecules in hydrophobic chromatography or biomembranes

Kosta Makrodimitris[ab]; Erik J. Fernandez[a]; Thomas B. Woolf[b]; John P. O'connell[a]
[a] Department of Chemical Engineering, University of Virginia, Charlottesville, VA, USA [b] Departments of Physiology, Biophysics and Biophysical Chemistry, and Biomedical Engineering, Johns Hopkins University, Baltimore, MD, USA

To cite this Article Makrodimitris, Kosta , Fernandez, Erik J. , Woolf, Thomas B. and O'connell, John P.(2005) 'ALLD: An object-oriented mesoscopic simulation program for polar biomolecules in hydrophobic chromatography or biomembranes', Molecular Simulation, 31: 9, 623 — 636
To link to this Article: DOI: 10.1080/08927020500108262
URL: http://dx.doi.org/10.1080/08927020500108262

Molecular Simulation, Vol. 31, No. 9, August 2005, 623–636

Taylor & Francis
Taylor & Francis Group

ALLD: An object-oriented mesoscopic simulation program for polar biomolecules in hydrophobic chromatography or biomembranes

KOSTA MAKRODIMITRIS†,‡*, ERIK J. FERNANDEZ†, THOMAS B. WOOLF‡ and JOHN P. O'CONNELL†

†Department of Chemical Engineering, University of Virginia, Charlottesville, VA 22904, USA
‡Departments of Physiology, Biophysics and Biophysical Chemistry, and Biomedical Engineering, Johns Hopkins University, Baltimore, MD 21205, USA

(Received November 2004; in final form January 2005)

The ALLD simulation software implements a mesoscopic lattice method to model hydrophobic chromatographic systems and biomembranes. The basis and some initial results of these applications emphasizing reversed phase chromatography of peptides are reviewed. The program structure and coding are described along with concepts for parallelization to simulate massive systems and large biomolecules. Extensions of the method for simulations with variable temperature, solute and solvent polarization, effects of ionized solutes and added salts and heterogeneous media are presented.

Keywords: Mesoscopic simulation; Biomolecules; Hydrophobic chromatography; Biomembranes

1. Introduction

A mesoscopic simulation environment [1,2] has been developed based on a Langevin lattice approach [3–5] in order to study the adsorption and interactions of biomolecules in biomembranes and in hydrophobic chromatography systems. Membrane proteins are involved in many important biological processes that include cell signaling and drug interactions [6]. An ability to understand how they move and fold to a stable tertiary structure would be especially valuable due to the difficulties in obtaining good crystals for X-ray studies and the current challenges in solid-state NMR for membrane proteins. Hydrophobic chromatography (RPC, HIC) has many applications that include the downstream purification of proteins for industry [9]. It is also an excellent tool to study the interactions and hydrophobicity of amino acids [10].

All-atom simulations that explicitly include the biomembrane and surrounding water along with protein, have shown the importance of an understanding of the solvation setting for determining protein behavior [7,8]. There have been several simulation studies to try and predict the behavior of proteins and peptides in RPC/HIC systems [11–15]. In these, either a highly simplified mean-field model for the solvent was adapted or a very detailed all-atom view with poor sampling for thermodynamic properties was applied. These studies suggest the need for a mesoscopic simulation method that can capture behavior on a longer time-scale for partitioning and sample events from a broader range of conformations and from a complex interfacial region. Thus, a good mesoscale model could dramatically impact conformational sampling and structure:function studies by improving understanding of protein behavior in both biomembranes and chromatography without requiring extreme amounts of computer time.

We believe it is important to develop a computational setting that is highly efficient and accurate enough in terms of predictive thermodynamics to be useful for chromatographic experimental design. For example, hydrophobicity scales [16] and modeling approaches such as solvophobic theory [17], preferential interaction theory [18] and lattice models based on polymer statistical mechanics [19] do not treat the 3D molecular structure of the solute and the orientations of the solute to the chromatographic surface in a fundamental way. Other approaches like molecular descriptors [20] account for the 3D molecular structure but do not consider orientational effects and cannot be connected directly to thermodynamic analyses and interpretation.

*Corresponding author. Tel.: +1-434-924-3393. Fax: +1-434-982-2658. Email: km4aa@virginia.edu

Molecular Simulation
ISSN 0892-7022 print/ISSN 1029-0435 online © 2005 Taylor & Francis Group Ltd
http://www.tandf.co.uk/journals
DOI: 10.1080/08927020500108262

The ALLD method is intended to perform the following computations in minimum CPU time: (1) Predict adsorption equilibrium quantitatively, (2) Describe variations of mobile and stationary phase constitutions, (3) Include the 3D structure of the solute in detail, (4) Determine preferable orientations, (5) Analyze the energy and entropy of interactions and driving forces, and (6) Model hydrophobic chromatography systems.

2. Theory of polarization and the Langevin function

In order to study the mechanisms, with which atoms and polar molecules respond to an electrical field, i.e. to gain insights into the mechanisms leading to the formation and/or orientation of dipoles we need a general theory of polarization [21]. There are essentially four basic kinds of polarization mechanisms:

- Interfacial polarization: charged surfaces and interfacial boundaries orient dipoles in the direction of their external fields
- Electronic or atomic polarization: electrical fields displace the center of charge of electrons with respect to the nucleus and thus induce dipole moments
- Ionic polarization: external fields induce net dipoles in a solid material (internal dipoles) by slightly displacing the ions from their rest position.
- Orientational polarization: external fields align dipoles of asymmetric molecules in a fluid from their equilibrium random orientations

The macroscopic definition of polarizability associated with a specific material is:

$$\mathbf{P} = \varepsilon_0 \cdot \chi \cdot \mathbf{E} \tag{1}$$

where ε_0 is the permittivity constant of vacuum, $\mathbf{E}$ is the external electric field, and χ is the dielectric susceptibility.

This is an empirical equation implying a linear relationship between the applied field and the polarization. In order to describe the bulk material microscopically we sum up all individual dipole moment vectors $\boldsymbol{\mu}$ contained in the given volume of the material and divide this sum by the volume V. This gives us the (volume independent) polarization $\mathbf{P}$ of the material.

$$\mathbf{P} = \frac{\sum \boldsymbol{\mu}}{V} = \langle \boldsymbol{\mu} \rangle \cdot N_V \tag{2}$$

where N_V is the density of dipoles.

The effect of an electrical field on randomly distributed dipole moment vectors is twofold:

(1) partially aligns permanent dipoles in the direction of the field
(2) induces dipoles in the material and partially aligns them in the direction of the field

In the case of orientation polarization, the mean electric dipole moment is estimated by a calculation similar to that of Langevin [3] to find the magnetic moment of gas molecules with permanent magnetic moments.

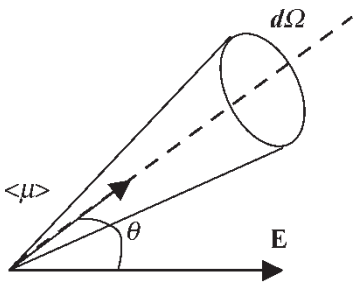

Figure 1. Orientation of the dipole in the presence of the field where θ is the angle between the dipole and the field and the dipoles are confined within solid angle dΩ.

The potential energy of a dipole μ in a field E is given by

$$U = \boldsymbol{\mu} \cdot \mathbf{E} = \mu E \cos\theta \tag{3}$$

where θ is the angle between the dipole and the field is as shown in figure 1.

In order to find the average moment $\langle \boldsymbol{\mu} \rangle$ in the direction of the field of one molecule, Debye [4] used the expression:

$$\langle \boldsymbol{\mu} \rangle = \frac{\int A e^{(\mu E)/(k_B T)} \boldsymbol{\mu} \cos\theta \, \mathrm{d}\Omega}{\int A e^{(\mu E)/(k_B T)} \mathrm{d}\Omega} \tag{4}$$

where A dΩ is the number of dipoles pointing in the directions confined within the solid angle dΩ.

When an electric field $\mathbf{E}$ is applied to a system of molecules having dipole moment $\boldsymbol{\mu}$, there is a torque $\boldsymbol{\mu} \times \mathbf{E}$ tending to align their dipoles with the field. However, thermal agitation tends to randomize the dipole orientations. Langevin applied the Boltzmann distribution law for this classical system of independent dipoles in order to find the relative probability of the orientation being in the solid angle dΩ and obtain the system Gibbs energy. Equation (4) becomes

$$\frac{\langle \boldsymbol{\mu} \rangle}{\boldsymbol{\mu}} = \frac{1}{\tanh(y_L)} - \frac{1}{y_L} = L(y_L) \tag{5}$$

where the Langevin argument is

$$y_L = \frac{\mu E}{k_B T} \tag{6}$$

Figure 2 shows the Langevin function $L(y_L)$ of equation (5). Deviations from linearity appear when saturation effects become appreciable for $y_L > 1$, and the function at infinite intensity is unity, $L(\infty) = 1$.

Fortunately experimental conditions are often such that y_L is small enough for linear behavior

$$\lim_{y_L \to 0} L(y_L) = \frac{y_L}{3} \tag{7}$$

3. ALLD methodology

Solutes are represented atomistically by a combination of partial charges obtained from an atomistic forcefield.

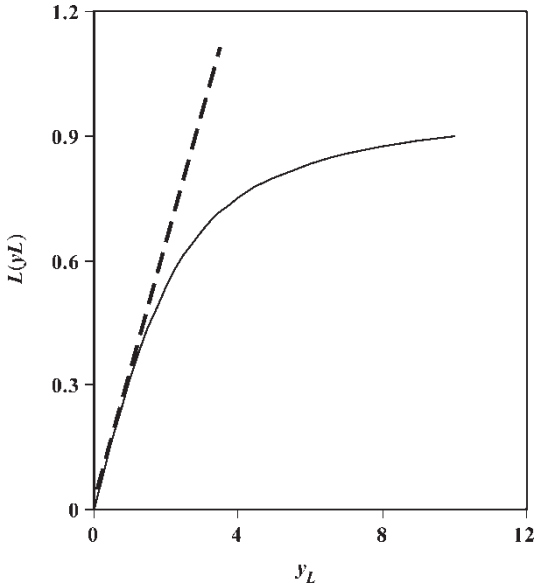

Figure 2. Plot of Langevin function; linear at low intensities and saturated at very large fields.

Figure 3 illustrates the three states in the ALLD simulations that affect the values, directions and the number of the dipole vector points:

(1) A grid of dipole vectors in the rectangular simulation box
(2) A cavity within the lattice for the solute to occupy
(3) A solute placed in the cavity and whose partial charges create an electric field, to which the dipoles respond with changes in values and directions.

The solvation free energy change from state 1–3 is written as a sum of a cavity term for the change from state 1 to state 2 and three terms of electrostatics, dipole reorientation and overlap (repulsion) if the solute interacts with a boundary such as the surface of hydrophobic media. The free energy of adsorption is determined from the difference between the free energy value found for this change of states in only solvent and that found in the interfacial region [2].

3.1. Solvent representation

Lattice-dipole models use variable dipole vectors placed in random directions at specified grid points in order to represent the environment before a solute is inserted into the system. In adsorption, if the interface is nonpolar, the lattice dipole moments decrease from the solvent to the surface. The dipole profiles with position generally appear as in figure 4 for hydrophobic chromatography and biomembrane systems. A membrane bilayer is conceived as hydrophobic chromatography interface and its mirror profile except that the solutes may pass through the biomembrane and not into the chromatography substrate. Thus it is appropriate to study both kinds of systems using similar approaches.

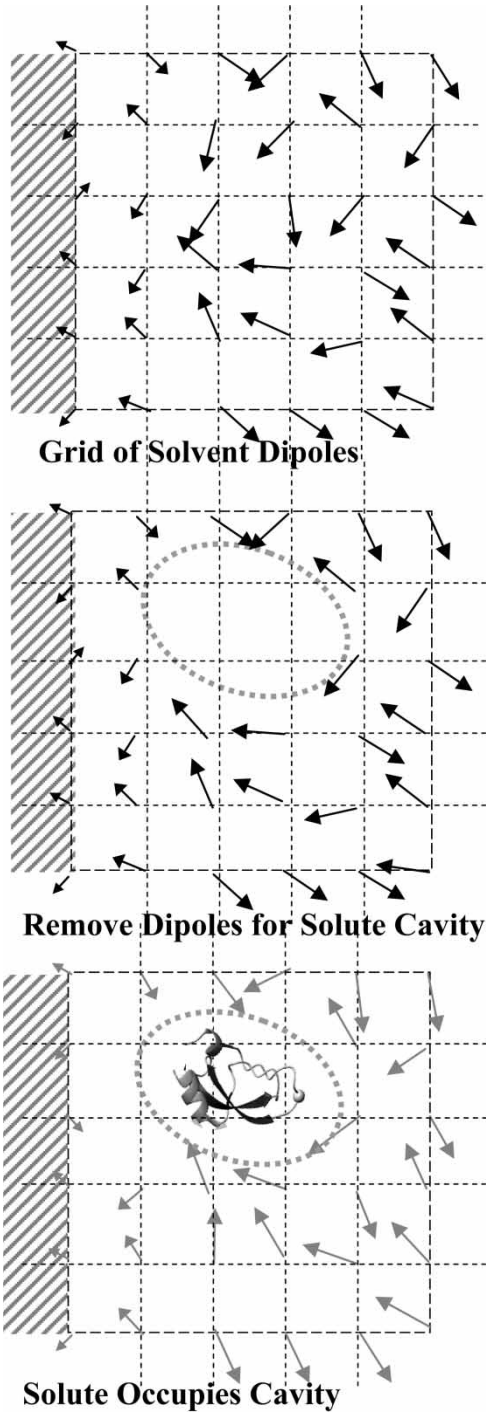

Figure 3. Representation of the three states of ALLD method.

Our focus is on chromatography, so we modified the expression for the dipole profile by Grossfield, *et al.* [1] for biomembranes. Their dipole profile for biomembranes in the Z direction was

$$\mu_i = \frac{\mu_\infty - \mu_0}{2}\left[\tanh\left(\frac{|Z_i| - A}{B}\right) + 1\right] + \mu_0 \qquad \text{(8a)}$$

(*biomembrane*)

where Z_i is the position of dipole i, μ_∞ is the dipole in the solvent (asymptote) and μ_0 is the dipole moment at

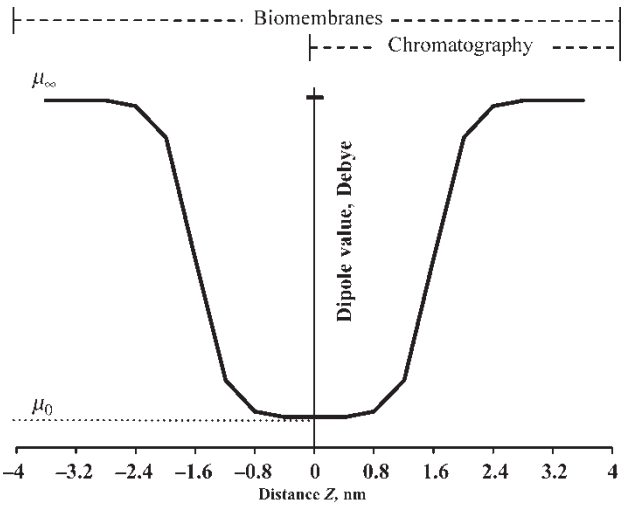

Figure 4. ALLD dipole profiles of a biomembrane and of hydrophobic chromatographic system.

the membrane center line. The parameter A sets the Z value at the half-height and B sets the steepness. For chromatography we use

$$\mu_i = \frac{\mu_\infty - \mu_0}{2}\left[\tanh\left(\frac{Z_i - A}{B}\right) + 1\right] + \mu_0 \quad \text{(8b)}$$

(*chromatography*)

The dependence of the function (8b) on the parameters A and B is shown in figure 5 showing that it is symmetric about the half-height. We use $A = 1.6$ nm and $B = 0.4$ nm in a rectangular simulation box with edges at $L_x = L_y = 3.2$ nm and $L_z = 6.4$ nm. As with Grossfield, *et al.* when creating the cavity, a dipole was removed from a lattice point if the center of any atom of the solute would be closer than 0.2 nm to the point.

3.2. Solute representation

Solute peptide structures can be based on X-ray crystal structures, modeled as ideal a-helical structures, or directly used as the minimum energy configuration from a molecular utility. Grossfield, *et al.* used the AMBER forcefield [22] to study model cases such as amino acid side analogs and small WALP peptides interacting with biomembranes. We have employed the CHARMM forcefield [23] for atomistic representation of the amino acid structure of peptide solutes in hydrophobic chromatography. Some of the peptides had protected groups such as $-NO_2$ that were not amino acids, and thus not represented in the CHARMM program. For these, we used the partial-bond-charge increment method of the Merck molecular force field [24]. It is based on formal charges, atom types, electronegativities, bond lengths and bonded neighbors of the force field in order to assign partial charges in groups and atoms that CHARMM, AMBER or other force fields do not treat.

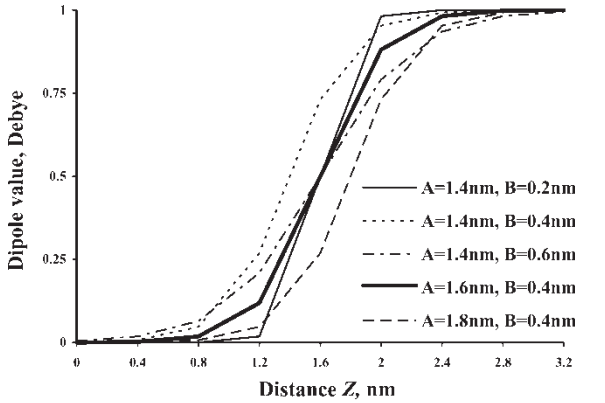

Figure 5. Dependence of the dipole permanent profile function on the parameters A and B of equation (8b).

4. Chemical potential energy terms

4.1. Cavity term

The chemical potential change from replacement of solvent by solute is rigorously a complex function of size and interaction effects, especially in aqueous solvents. It is common to use van der Waals sizes and surface areas to estimate this term, but this introduces additional parameters and is not always successful [17]. Following Grossfield, *et al.* [1] we have modeled this term as a Keesom energy [25] for interactions of permanent dipoles in the absence of solute, μ_0, that are replaced by the solute (*Excl*) and those, which remain (*Incl*) [2].

$$\Delta G^0_{\text{cavity}} = \sum_i^{\text{Excl}} \sum_j^{\text{Incl}} \frac{2\mu^2_{0,i}\mu^2_{0,j}}{3k_BT(4\pi\varepsilon_0)^2 r^6_{ij}} \quad (9)$$

where ε_0 is the dielectric permittivity of vacuum.

This term is taken from the potential of mean force between two permanent dipoles at constant temperature (Keesom, 1921). The solvent lattice dipoles are permanent dipoles, and interact favorably with the surrounding dipoles, even in the absence of solute partial charges (electric field) to orient them.

4.2. Electrostatic term

For a rigid, nonpolarizable solute, the electrostatic chemical potential difference is estimated from changes in the electrostatic field by insertion of the solute's charges and dipoles into the cavity

$$\Delta G^0_{\text{electro}} = -\sum_j^{\text{Incl}} \boldsymbol{\mu}_j \cdot \mathbf{E}^0_j \quad (10)$$

where $\boldsymbol{\mu}_j$ is the final dipole at the lattice point j.

Since each solvent dipole is influenced by the other solvent dipoles, it is necessary to do an iterative calculation to arrive at dipole values and orientations for state 3 that are electrostatically consistent with the solute's

field. On lattice point j at iteration n, the magnitude and the orientation of the electric field, and the dipole moment, are found via the following equations [2]

$$\mathbf{E}_j^0 = \sum_i^{\text{peptide}} \frac{q_i \mathbf{r}_{ij}}{r_{ij}^3} \tag{11}$$

$$\boldsymbol{\mu}_j^1 = \mu_{0j} \hat{\mathbf{E}}_j^0 \left[L(y_L)\right] \tag{12}$$

$$\mathbf{E}_j^n = -\nabla\phi(\mathbf{r}_j)^n = \mathbf{E}_j^0 + \sum_{j\neq k} \frac{3(\boldsymbol{\mu}_j^n \cdot \mathbf{r}_{jk})\cdot \mathbf{r}_{jk}}{r_{jk}^5} - \frac{\boldsymbol{\mu}_j^n}{r_{jk}^3} \tag{13}$$

$$\boldsymbol{\mu}_j^{n+1} = \alpha \cdot \boldsymbol{\mu}_j^n + (1-\alpha)\cdot \mu_{0j} \hat{\mathbf{E}}_j^n \left[L(y)\right]^n \tag{14}$$

where r_{ij} and r_{jk} are the distances of separation of the charges from dipoles and of the dipoles from each other; q_i is the partial charge i in the solute according to the CHARMM, MERCK, or AMBER force fields; $\mu_j^n$is the lattice dipole j of the solvent at iteration n and α is an iteration control parameter and relaxation factor for the numerical scheme.

4.3. Dipole reorientation term

There is an effect due to the lattice dipoles changing their average orientation when a solute is inserted. In the Langevin lattice, the partition function is [1]

$$Q(N,V,\beta) = \int e^{-U(\mathbf{E},\boldsymbol{\mu})/k_B T} \mathrm{d}\boldsymbol{\mu} = \int e^{-y_L} \mathrm{d}y$$

$$= \frac{4\pi}{y_L} \sinh(y_L) \tag{15}$$

The energy is unchanged in this case, but there is an entropy effect of [2]

$$\Delta S_r = S - S_0$$

$$= k_B[-y_L \coth(y_L) + \ln(\sinh(y_L))$$

$$- \ln(y_L) + 1] \tag{16}$$

for a solute replacing the solvent with y changing from zero to the converged value.

The system of equations (10)–(14) and (16) is solved iteratively until

$$\frac{|(\Delta G_{\text{electro}} - T\Delta S_r)^n - (\Delta G_{\text{electro}} - T\Delta S_r)^{n-1}|}{(\Delta G_{\text{electro}} - T\Delta S_r)^n}$$

$$< 0.5\% \tag{17}$$

4.4. Repulsive term

The repulsion energy due to overlap forces on a solute near the chromatography surface has been estimated by [25]

$$U_{wall} = \sum_i^{\text{charges}} \frac{\pi \rho_i \varepsilon_i \sigma_i^{12}}{45(z_i + S_d)^9} \tag{18}$$

where the packing factor is $\rho_i = \sqrt{2}/\sigma_i^3$ (close packed solid), σ_i is the van der Waals radius of solute atom i and ε_i is an energy parameter. The values for σ_i were taken from Bondi [26] while values for ε_i were taken from Daragan and Mayo [27]. The inverse 9th power arises from the inverse 12th power repulsive term between 2 atoms (Lennard-Jones term) assuming pairwise additivity at the interaction energies of atoms and the planar surface of the solid [25].

The total free energy change for replacing solvent dipoles with solute is

$$\Delta G_Z = \Delta G_{\text{electro}} + \Delta G_{\text{cavity}} - T(\Delta S_r) + U_{\text{wall}} \tag{19}$$

5. Orientations and averaging for comparison with experiment

To establish solute orientation, its coordinate axes are defined with a z-axis from the center of solute geometry to the atom furthest from the center and the x and y axes are arbitrarily defined normal to z. Different alignments may be examined to evaluate possible preferential orientations for solute adsorption as shown in figure 6. To obtain average values at the given Z location and for different z–Z alignments, calculations were performed at different rotational increments about the z axis, since solute partial charges and dipoles would not be symmetrically positioned and thus have variable distances to lattice dipoles with rotation.

Orientational averaging was done via two methods:

$$\left\langle \Delta G_Z^0 \right\rangle = -k_B T \ln\left\{ \sum_i^{\text{orientations}} \exp\left(\frac{-\Delta G_Z^0}{k_B T}\right) \right\} \tag{20a}$$

and

$$\overline{\Delta G_Z^0} = \frac{\sum_i^{\text{orientations}} \Delta G_Z^0 \exp\left(\frac{-\Delta G_Z^0}{k_B T}\right)}{\sum_i \exp\left(\frac{-\Delta G_Z^0}{k_B T}\right)} \tag{20b}$$

As noted by Davidson [28], these two averages should be numerically the same if proper sampling is made of a system with small fluctuations.

In the present case, $\overline{\Delta G_Z^0}$ calculations were done at 14 unique orthogonal alignments of each of the solute Cartesian coordinate vectors $\mathbf{e}_x$, $\mathbf{e}_y$, $\mathbf{e}_z$ at angles of $n\pi/4 (n = 0, 1, 2)$ radians relative to the Z-lattice axis. Tests were done for several peptides with one to ten z–Z alignments in order to see where the simulated adsorption equilibrium constants reached a plateau and the orientationally averaged results did not change significantly with additional alignments as shown in figure 7. Eight rotational positions about the z-axis were the set chosen as the minimum number needed since more orientations would not change the results. So, at each of 14 orientations, calculations were made at 8 unique rotational positions about the z-axis at every $\pi/16$ radians for a total

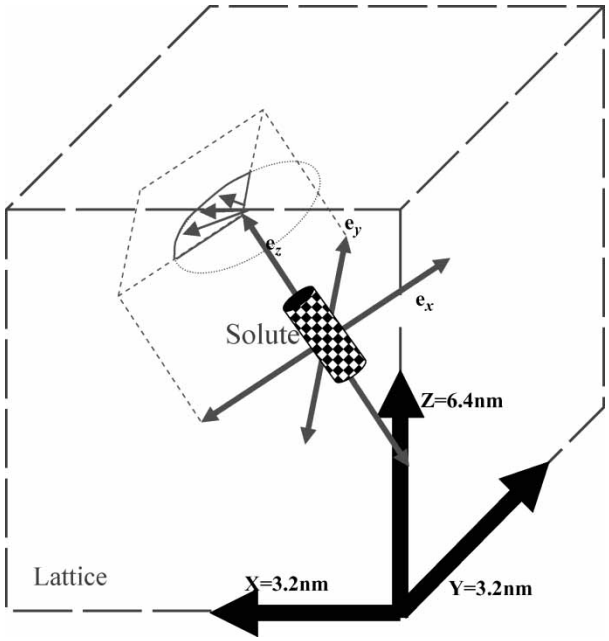

Figure 6. Alignment of peptide solute x, y and z internal axes relative to solvent dipole lattice X, Y, Z axes.

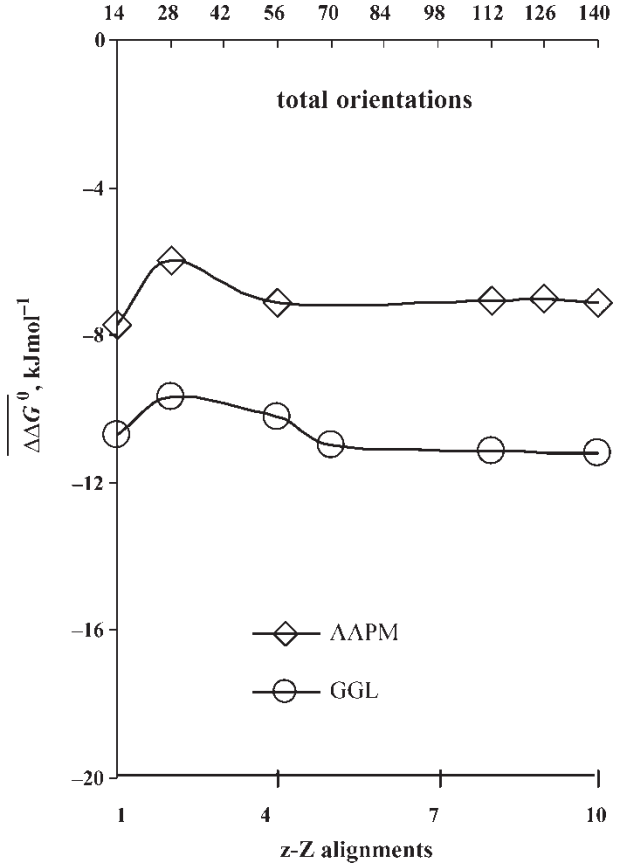

Figure 7. Dependence of the averaged chemical potential differences on the z–Z alignments and the total number of orientations.

of 112 orientations. The 4-fold symmetry of the cubic lattice representation was utilized in obtaining the values.

As an example of orientation dependence, figures 8a,b,c,d shows 4 sets of Z variations of in the 14 orientations for the peptide VY at four sequential z–Z alignments every $\pi/8$. Several orientations have a minimum with negative ΔG_Z^0 as a function of Z, while others do not.

Figure 9 shows Z-profiles of the four contributions (electrostatics, entropy, cavity and repulsion) to ΔG_Z^0 for the VY peptide in hydrophobic chromatography. All contributions but the repulsion are asymptotic to zero at the substrate surface and to fixed values at large separations (only solvent environment). While repulsion alone might determine the closest approach to the substrate, all of the other terms actually establish a minimum location and value. The magnitude of the electrostatic term is largest, while the range of variation of the cavity term is the longest.

The standard adsorption chemical potential at a given location Z, $\Delta\Delta G_Z^0$, is the difference in the orientation-average at the position Z from that at $Z = \infty$ (in solvent only). For example, for equation (20b)

$$\overline{\Delta\Delta G_Z^0} = \overline{\Delta G_Z^0} - \overline{\Delta G_\infty^0} \tag{21}$$

This quantity is to be compared with experiment.

Calculations were also made with the averaging form (20a) to find $\langle \Delta G_Z^0 \rangle$. Differences were found for some peptides, as described below. We are currently revaluating the set of orientations to be used to arrive at final values for fitting and comparison.

6. Results and discussion

Grossfield, *et al.* [1] used the Langevin dipole method to calculate electrostatic interactions in a heterogeneous membrane environment. Their Langevin model had three parameters: the dipole moment for dipoles in the hydrophobic core of the biomembrane, μ_0, the dipole moment for solutes in the aqueous region, μ_∞ and a multiplier for the cavity term. These parameters were chosen to reproduce transfer free energies for side chain analogs from bulk hydrocarbons to water. The parameterization was performed through an extensive scheme of adjusting side chain analog conformations to fit experimental transfer free energies. A series of test cases were presented and the model produced qualitatively correct results when applied to a variety of molecules interacting with membranes, including simple charges and dipoles, side chain analogs and helical peptides.

We have revised the ALLD method to apply to adsorption of protected peptides in reversed phase chromatography and made comparisons of experiment and calculation [2]. In particular, we reduced the unknown parameters to a single quantity, μ_∞, by removing the cavity multiplier and setting $\mu_0 = 0$.

Experimental standard free energy (or chemical potential) differences between the mobile and stationary phases were calculated from equilibrium constants, K, obtained from retention data

$$\Delta\overline{G}^0 = RT\ln K = RT\ln\left(\frac{V_r - V_0}{V - V_0 - V_{\text{excol}}}\right) \tag{22}$$

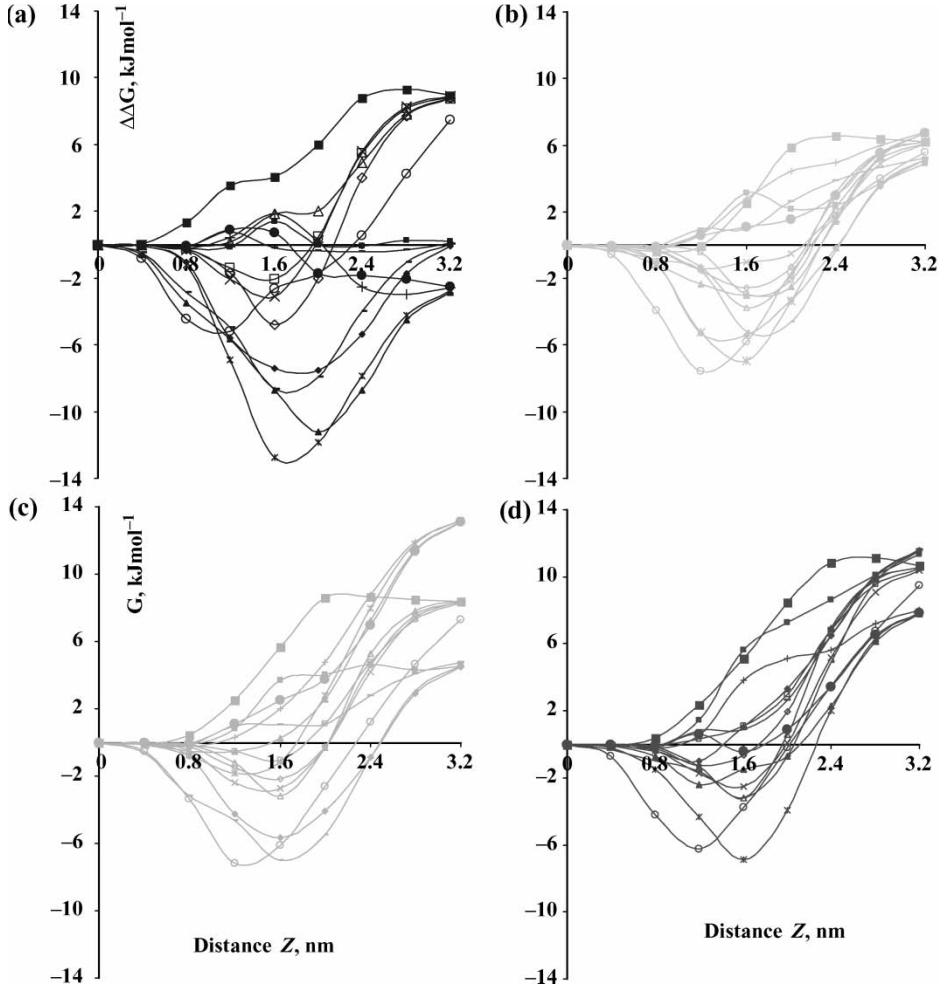

Figure 8. Z variations of the chemical potential in the 14 $X-Y$ orientations for the peptide **VY** at four sequential $z-Z$ alignments every $\pi/8$.

where V_r is the volume, at which the peptide elutes, V_0 is the volume when a nonadsorbing tracer elutes, V is the volume of the bed container and V_{excol} is the volume of the container not occupied by the adsorption media.

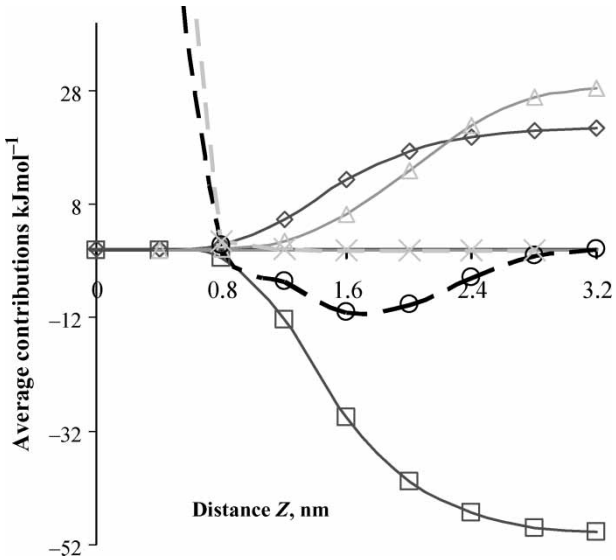

Figure 9. Angle-averaged contributions (Eq. 206) to computed standard free energy difference for the MLP peptide. (□) Electrostatic; (◇) Reorientation; (Δ) Cavity; (X) Repulsion; (○) Total.

Nine protected peptides covering a wide range of hydrophobic characteristics such as structure, retention and hydrophobicity, and of practical retention volumes were chosen. Adsorption properties of these peptides are shown in table 1, ordered from low to high equilibrium constant by indexes from one to nine. (Recent remeasurement of these peptides gave a revised value for 3-PL; it is now indexed one instead of three as previously [2]). Table 1 also lists peptide properties of the Meek [16] hydrophobicity scale value (HS), the radius of gyration (RG), the accessible hydrophobic surface area (HSA), the molecular volume (MV), the dipole moment (DM) and the number of atoms.

In all our calculations $\overline{\Delta\Delta G^0_Z}$ showed a minimum at some position $Z_{\min}$. Comparisons were made with $\overline{\Delta\Delta G^0_{Z\,\min}}$ at its minimum for different solvent dipoles, μ_∞. The value of $\mu_\infty = 1.06$ gave agreement with the experimental value for adsorption of **VY** (index 5) for both $\langle\Delta\Delta G^0_Z\rangle$ and $\Delta\Delta G^0_Z$. Once this value was fit, all quantities in equations (10–15) were unchanged and only the CHARMM forcefield representation of the peptides varied in the comparisons. Figure 10 shows that experiment and simulations for both forms of averaging. The magnitude and retention strength are generally followed, but some differences in averaging are too large to determine how

Table 1. Protected peptide formulae, experimental results and properties.

PROTECTED PEPTIDE	Index	K (equation 21)	$\Delta\overline{G}^0$ ($kJ\,mol^{-1}$) (equation 21)	HS	RG (nm)	HAS (nm^2)	MV (nm^3)	MD (debye)	atoms
Z-Pro-Leu-Gly-amide (3-PL)	1	7.4	− 4.9*	49.44	0.44	6.86	0.41	3.37	60
N-Methoxysuccinyl-Ala-Ala-Pro-Val-p-nitroanilide (AAPV)	2	7.5	− 5.0	23.52	0.63	9.23	0.56	1.87	80
N-Methoxysuccinyl-Ala-Ala-Pro-Met-p-nitroanilide (AAPM)	3	9.6	− 5.6	31.57	0.66	9.68	0.57	3.52	81
Z-Met-Gly-ethyl ester (MG)	4	18.4	− 7.2	27.97	0.47	6.98	0.36	5.02	49
Z-Val-Tyr-methyl ester (VY)	5	30.7	− 8.5	41.53	0.56	7.69	0.43	3.27	59
pGlu-Phe-Leu-p-nitroanilide (FL)	6	35.3	− 8.8	58.47	0.51	8.10	0.48	3.40	68
Boc-b-Ala-Trp-Met-Asp-Phe-amide (AWMDF)	7	35.9	− 8.9	59.18	0.67	10.63	0.73	1.91	103
Z-Gly-Gly-Leu-p-nitroanilide (GGL)	8	99.5	− 11.4	25.42	0.47	7.34	0.46	5.68	65
N-Formyl-Met-Leu-Phe-benzyl ester (MLF)	9	157.0	− 12.5	87.57	0.49	8.20	0.53	5.55	74

*Remeasured value; changed from [2].

quantitatively accurate the predictions are. We are studying this issue in greater depth to develop a consistent and reliable averaging procedure.

The influence of solvent dipole difference, $\mu_\infty - \mu_0$, on ΔG^0 is indicated in figure 11 for butane and of μ_∞ on $\Delta\Delta G^0_{Z\,min}$ in figure 12 for VY. When the solvent dipole is decreased, the adsorption is less strong, with high sensitivity of $\Delta\Delta G^0_{Z\,min}$ to μ_∞. This suggests that the method could also predict desorption as a less polar solvent responds less attractively to the solute field, as would occur with added cosolvents for elution in hydrophobic chromatography.

The relative absolute contributions for the cavity, electrostatic and reorientation terms at Z_{min} are shown in figure 13 for all nine peptides. While the reorientation terms make about the same relative contributions in all cases, the cavity and electrostatic contributions cover a considerable range due to size differences and to electrostatic effects due to size and charge differences [2].

Figure 14 shows molecular structures for two orientations, (a) #13 that is unfavorable for adsorption, and (b) #2 that is favorable. The difference is the nonpolar surface and polar solvent environments of the amino acids Tyrosine (polar) and Valine (nonpolar). Thus, preferable orientations can be elucidated with ALLD.

To examine the influence of temperature on the results, we have calculated $\Delta\Delta G^0_{Z\,min}$ for VY at 293, 298, 313 and 328 K and compared it with experiment [29]. The results are linear in temperature suggesting that ΔS^0 is constant, the retention is exothermic and enthalpy driven, and that ΔCp^0 is small. Both the electrostatic and cavity terms yield enthalpy and entropy contributions [2,29]. We also find that fitted values of μ_∞ are a linear function of acetonitrile concentration in the solvent [29].

7. ALLD object oriented programming style

A way to describe software is through flowcharts and Unified Modeling Language (UML) [30].

The idea behind UML is that it can be used for modeling any type of information, not just in object-oriented systems. When one uses UML to design a system, the Computer Aided Software Engineering (CASE) tool typically specifies all objects and describes classes in static and dynamic ways. Figure 15 shows a UML *static class*

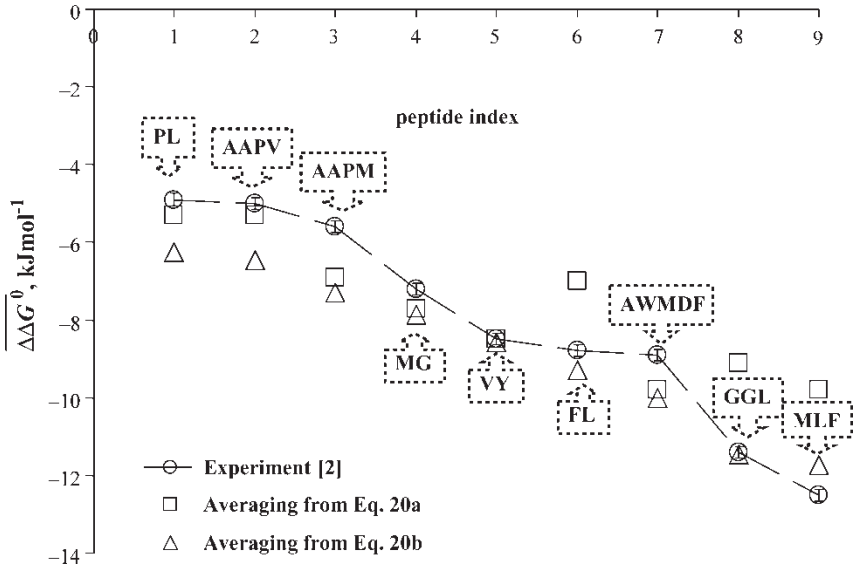

Figure 10. Comparisons of simulation free energy differences from different average with experimental adsorption free energies.

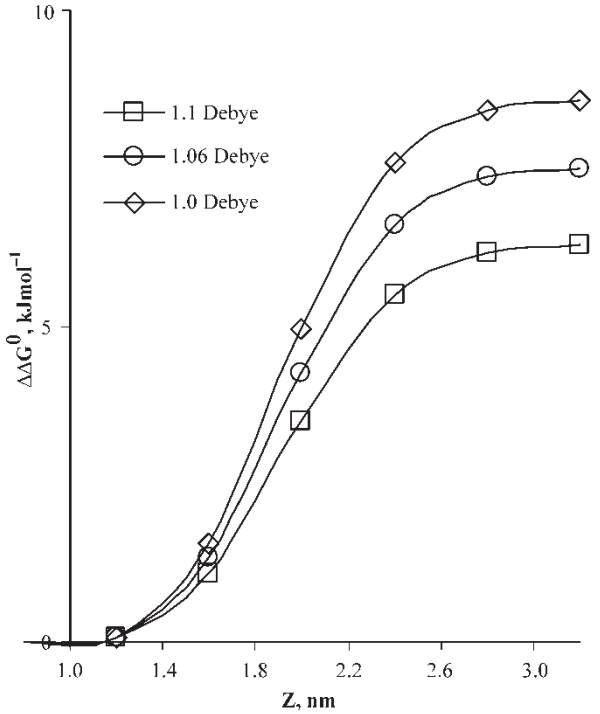

Figure 11. Free energy dependence, on position of n-butane as a function of asymptotic solvent dipole moment.

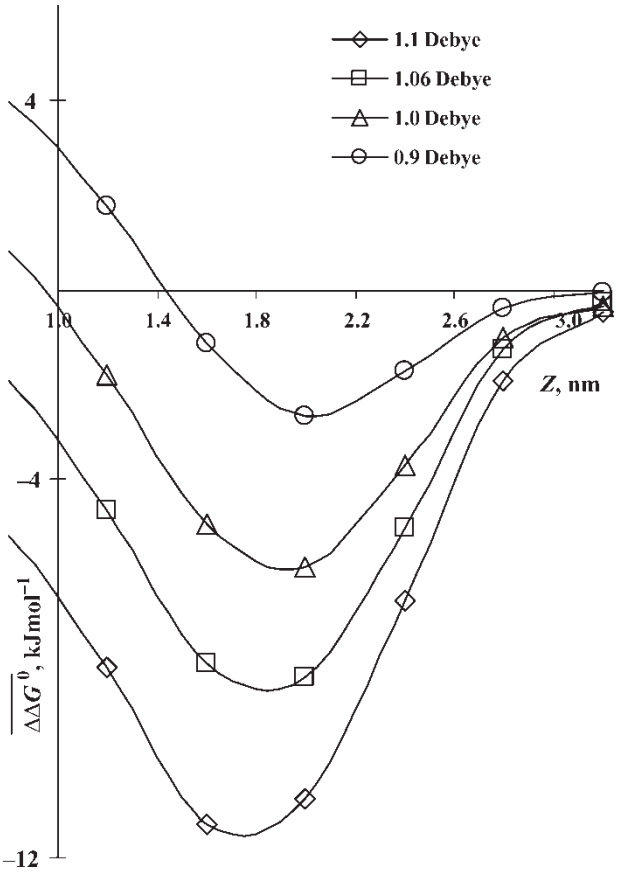

Figure 12. Free energy dependence on position of **VY** peptide as a function of asymptotic solvent dipole moment.

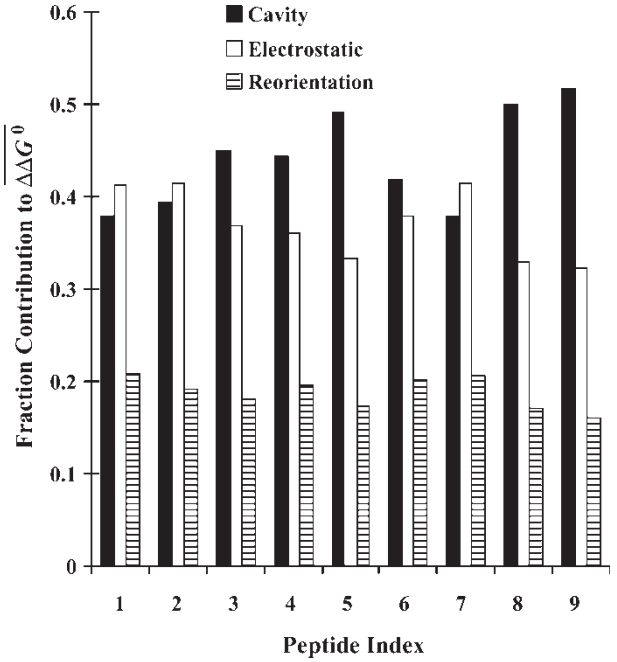

Figure 13. Fractional contributions of absolute values of electrostatic (< 0), cavity (> 0) and reorientation (> 0) terms to free energy of adsorption for 9 peptides.

diagram of the ALLD methodology. The notation here is that all names in CAPTIALS are classes and all names beginning with a Capital are functions.

All classes are driven in the software by the main class function DRIVE that carries the parameters; selects the specific options; globally implements the mathematical libraries; creates, allocates and deletes large multidimensional arrays; and performs parallelization of the code.

There are 9 classes, which are positioned as indicated in figure 15 where the first four classes are nested while the others are external:

- VECTOR (defines vectors and operations among them)
- TENSOR (defines tensors, matrices or sequences of vectors and operations among them)
- TRANSFORM-GEOMETRY (makes rotations, translations, alignments, gyrations and other geometric calculations and transformations of arrays)
- ENERGY-FIELD (defines potential, field and energy calculations for charges and dipoles)
- DIPOLE PROFILE (defines Langevin dipoles, calculates dipoles and dipole profiles)
- DIELECTRIC PROFILE (defines dielectric and salt concentration profiles using the method of Booth [31] to estimate the dielectric constant from the dipoles)
- IN-INITIAL (defines dipole grid and reads the partial charges, van der Waals radii, atom types and other solute properties)
- CONVERGENCE (defines convergence schemes for dipole-electric field coupled ALLD equations, solute polarization induction terms and coupled equations for the Nernst-Poisson-Boltzmann potential with charges)

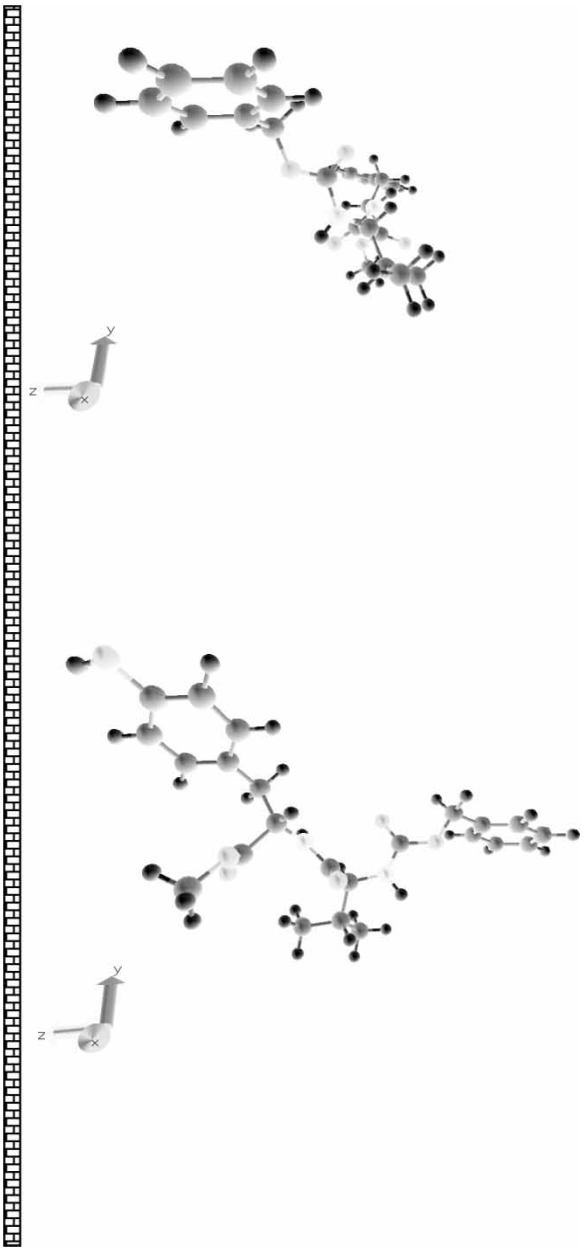

Figure 14. Unfavorable (top) and favorable (bottom) orientations of **VY** peptide toward a hydrophobic surface at left.

- WRITE (defines functions to write results for the energy terms, parameters and cases that have been studied, as well as values for fields, charges and dipoles during convergence)

The relations and interactions among classes are based on object-oriented principles. For example:

- *Inheritance* is a defining characteristic of the object-oriented language. TENSOR inherits functions from the VECTOR class and the ENERGY-FIELD class inherits properties and functions from the three ancestor classes it contains.
- *Polymorphism* is the property that a message can convey different meanings, depending on the object receiving it. For example, many operations in the VECTOR class have different meanings in the TENSOR class.
- *Encapsulation* of the information and clear definition of the interfaces must be implemented among all classes.

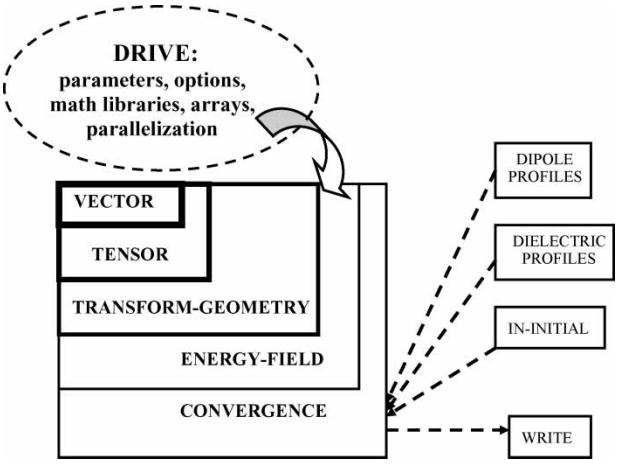

Figure 15. Diagram of ALLD object-oriented programming style.

In addition to static diagrams, there are UML dynamic class diagrams [30]. For each class there are diagrams:

- Case diagrams show the different individual functions in a generic sense (not as a C++ function) that the software package can perform. For example in ALLD, IN-INITIAL defines the function Build_grid(), which sets up the grid of dipole vectors to be used in the simulation box.
- Object diagrams describe instances of the classes. In ALLD, TRANSFORM-GEOMETRY instances appear and disappear during every rotation of the solute in the simulation box at every convergence step.
- Collaboration diagrams are where the program runs, and the code for an object member function might call a 'friend' member function in another object in another class. In ALLD, the function ALLD_converge_consistency() of the CONVERGENCE class could call the function Check_pro_after() in the WRITE class to write values for dipoles and fields and their contributions to the electrostatic term before and after convergence.

Post-processing of the results involves two importing steps: (1) putting files into Microsoft Excel worksheet templates where the representation of the chemical potential energy difference terms appears in colored graphs for orientations, angle averaging and interpolation. In this way it is possible not only to calculate energy minima and averages, but also to visually inspect the results for different orientations and translations along various axes; (2) giving different conformations and orientations in MOE modeling software [32] for studying preferable orientations at surfaces and interfaces.

8. Technical details and parallelization of ALLD method

The previous version of the Langevin lattice method to study the interactions of the peptides with biomembranes [1] was written in object-oriented style with the Python language as an extension of the MMTK python Molecular Dynamics software [33]. Although the development of the code was much easier (fewer code lines, friendly high level language) the speed was about 1/5 the current ALLD method and debugging and maintenance were difficult.

Our algorithm for the ALLD simulation method was developed in C^{++} with object-oriented programming style class hierarchy utilize its advantages in maintenance, inheritance, improvement and extension. We used the microsoft visual studio. NET C^{++} debugger and the microsoft developer network library http://msdn.microsoft.com/. The simulation runs were done with Microsoft C^{++}.NET 2003 (Windows XP OS), Intel C^{++} (Red Hat Linux OS) and The Portland Group C^{++} (Red Hat Linux OS) compilers. The hardware architecture was an Intel Xeon dual CPU at 2.8 GHz and a Linux cluster of 1.53 GHz AMD Athlon K7 MP CPUs. The runs for a specific case took a few hours, depending on the system and method. Simulation errors from the finite-sized lattice with limited number of the dipoles and the convergence scheme are estimated to be less than 1%.

9. Extensions of the ALLD method

9.1. Programming enhancements

Using the Message Passing Interface [34,35] parallel programming model for complex methods such as ALLD has some distinct advantages comparing to Directive-based programming interfaces (OpenMP). (See Appendix A for parallel strategies and MPI protocol.) There are three basic strategies [36] that could be implemented easily for parallelization of ALLD:

(1) *Cloning*: The Cloning model simply involves allocating P independent simulations to P independent processors, see figure 16. This technique is both easily implemented and very efficient but is limited in application. Though it is particularly suited to ALLD simulations, where each processor conducts, independent, translations along *Z*-axis or even rotations, this solution is always very expensive.
(2) *Master–Slave*: This model utilizes a master processor to run, or control the simulation. This processor allocates work to other processors when necessary, see figure 17. This model suffers from both communication difficulties and load balancing problems.
(3) *Replicated Data* (*Lattice Decomposition*): This model (see figure 18 and Appendix B for details) is based on the replicated data strategy [36] where identical copies of the configuration data are on all the processors. Lattice decomposition involves a subgroup of ALLD lattice points being assigned to each processor and the processor computes fields and dipole vectors only on these lattice points. This method, although more efficient, suffers from high communication overhead and demands large RAM.
(4) *Hybrid Lattice Decomposition and Master–Slave*: This scheme makes one processor node the master node and the other nodes workers (see Appendix B for details). The master node drives the other nodes as well as collects and evaluates the data.

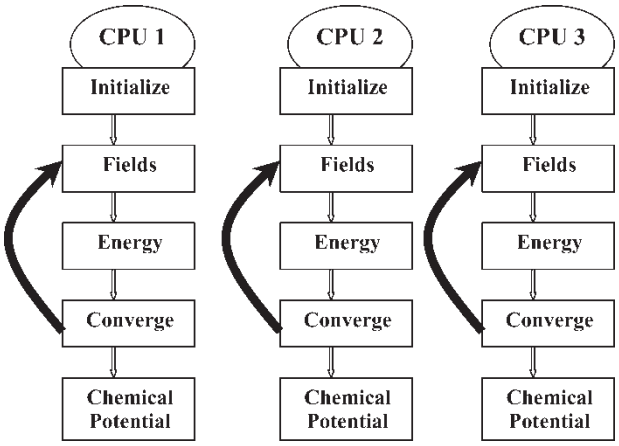

Figure 16. Cloning parallelization of ALLD method.

The ALLD code was written in C^{++} object-oriented style similar to that of NAMD molecular dynamics code [37] in order to enhance the interface between the methods. Linking ALLD and NAMD one could study the conformations of the solute [38], including appropriate averaging, and perhaps folding-unfolding equilibria of the proteins at different experimental conditions. Figure 19 is an example schematic for studying conformations with partial unfolding characteristics by coupling ALLD, NAMD and EXCEL, MOE visualization software.

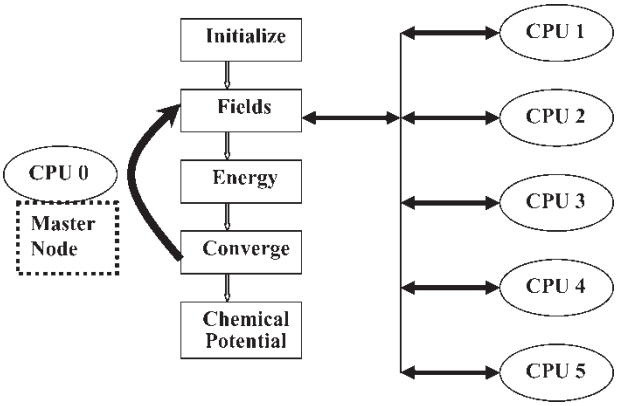

Figure 17. Master–Slave parallelization of ALLD method.

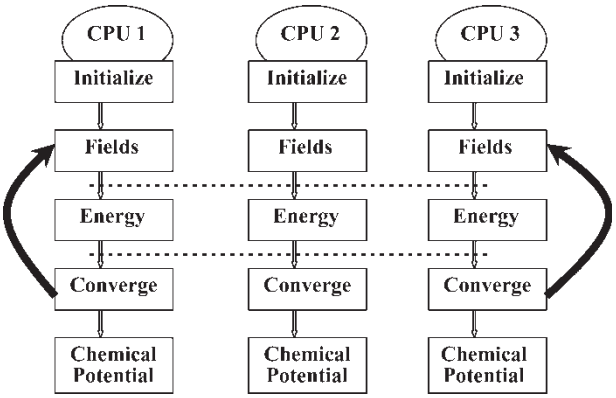

Figure 18. Replicated data parallelization of the ALLD method.

9.2. Heterogeneous surfaces and interfaces

One important advantage of the current lattice dipole methodology is its flexibility to adopt a variety of functions of dipole moments that might fully represent the microscopic polarity of a real-system solvent and the heterogeneity and 3D topology of interfaces. This would avoid the coarse assumptions of macroscopic parameters such as dielectric constant. Different modifications of equation (5) could be implemented along the Z-axis and nonuniform $X-Y$ lattice structures. Geometric and topological properties of the chromatographic porous adsorbents might be investigated using stochastic reconstruction methods [39] based on microscopic techniques and 2D images. Such structural data might be used for more realistic representations of the lattice especially where the repulsion term of equation (18) dominates.

9.3. Induction and van der Waals terms of solute dipoles

The (Langevin-lattice) dipole moments (LLD) of solvent molecules actually induce dipole moments on the atoms of the solute molecule according to

$$\boldsymbol{\mu}_i^{\text{induct}} = \alpha_i \mathbf{E}_i^{\text{LLD}} \tag{23}$$

The field $\mathbf{E}^{\text{LLD}}$ would then be calculated from both the interaction of the permanent dipoles of the solvents and the induced solute dipoles from the field and the solute atom polarizability. The contribution to the free energy of such solute-induced dipoles could be estimated by

$$\Delta G_{\text{solute}}^{\text{ind}} = -\frac{1}{2}\sum_{i}^{\text{solute}} \boldsymbol{\mu}_i^{\text{ind}} \cdot \mathbf{E}_i^{\text{LLD}} \tag{24}$$

Induction terms for LLD solvents could also be calculated, however the assignment of polarizability values for each lattice dipole is uncertain and would probably lead to additional parameters.

London dispersion terms could be calculated at infinity using parameters such as from Florian *et al.* [40] in order to account for the van der Waals contributions

$$\Delta G_{vdW} = -k_{vdW}\sum_{i}^{\text{solute}} C_i \left(\frac{\sigma_i^0}{r_{ij}}\right)^6 \tag{25}$$

where σ_i^0, C_i denote atomic vdW radii and London coefficients, respectively, and r_{ij} is the distance between the ith atom and the jth grid point. In the present calculations none of these terms have been included.

9.4. Salt effects

We have designed a Nernst-Poisson-Boltzmann (NPB) approach for combination with the ALLD method to study of added salt effects in hydrophobic chromatography [41]. The implementation involves two sequential convergence schemes for electrostatic dipole effects and for contributions from both solvent and ion ordering. In addition to the dipole lattice, there is a lattice of partial charges q_i and electrostatic potentials Φ_i at every grid point that must be converged to consistency with the equations:

$$\Phi_i = G(q_i, D_{ij}, r_{ij}) \Leftrightarrow q_i = F(\Phi_i) \tag{26}$$

where D_{ij} is the dielectric constant between the charges separated by distance r_{ij}. In addition to finding changes in solute adsorption, the formulation is intended to include enthalpy and entropy effects associated with the salt [42].

9.5. Forcefields based on multipole moments

In order to estimate the molecular electrostatic potential (MEP) of the solute, isotropic point-charge models have been used (AMBER, CHARMM) because of their ease of use and reliability. These forcefields are sensitive to sampling errors in their derivation, are not always transferable from the small molecules used in their generation to larger ones, and they are evaluated for only the single conformation put in.

Multipolar representations of charge densities (dipoles, quadrupoles, octupoles) could be used for electrostatic potential construction of the biomolecules for the ALLD method. A project is in progress to use multipoles from

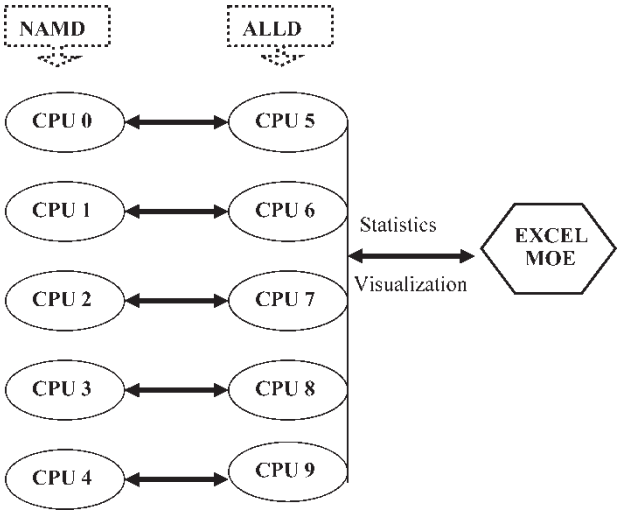

Figure 19. Structure of ALLD, NAMD and MOE software system for conformation studies of proteins.

the Theory of Atoms in Molecules and the Transferable Atom Equivalent (TAE) method [43]. TAE has been developed to provide electron densities, energies and properties that approach *ab initio* quality at minimal computational cost. It is expected that TAE multipoles can be used to approximate MEP distributions on molecular van der Waals surfaces including the effects of variable conformations [43].

Acknowledgements

The authors are grateful to Professor Curt Breneman and Dr. Alan Grossfield for useful discussions concerning the simulations and to the reviewer who raised the issues associated with angle averaging.

Appendix A: Parallel efficiency and MPI

In order to evaluate the efficiency of a parallel computing strategy one must handle the following issues:

- Load balancing (equally dividing work among processors and memory requirements)
- Communications (Minimizing the number of messages, maximizing information per message and local communicating rather than globally)

The purpose is to reduce the time per ALLD step, T_s:

$$T_s = T_p + T_c \tag{A1}$$

By minimizing both the processing time, T_p, and communication time, T_c, is for each step. In this way optimum elapsed time scaling with problem size and the best performance scaling with number of processors may be obtained.

It is best to insert the optimization code into the original serial code for communication between processes and data. The MPI protocol was developed from MPI Forum (1994) for several years in a collaboration of 60 scientists. The Message Passing Interface parallel programming model (MPI) [34,35] has advantages compared to Open MP, which has parallelization through directives and automatic communication through compilers. These are:

- Portability of programs to different hardware architectures
- Efficient implementation in both distributed and global shared memory systems
- High functionality and flexibility in the choice of communication and user-defined data types in complex software and massive calculations.

Appendix B: Replicated data and master–slave parallelization

- Replicated data (Lattice decomposition)

  The replicated data strategy [36] has identical copies of configuration data on all processors. Lattice decomposition involves a subgroup of points being assigned to each processor. In ALLD the processor computes fields and dipole vectors at only those lattice points. Though each processor has a complete copy of the coordinates, dipoles, charges and fields of the lattice grid points and the solute atoms, only a sub-block of the $N \times N$ matrix of interactions among the N lattice points is computed. Thus, each of the P processors would calculate only $N(N-1)/2P$ interactions. To complete the summation of the forces on each processor, the incomplete force arrays must be circulated to all the other processors. This "global pass-and-sum" strategy involves each processor exchanging its data (N/P of the data) with adjacent processors and summing the arrays, see figure 18. As every processor concurrently follows this sequence, the end result is an identical sum on all processors, and all of the original arrays are local to each processor.
- Hybrid lattice decomposition & master–slave

  A replicated data strategy could be used to make one processor node the master node and the others worker nodes of a parallel machine. The master node reads in all the data from the files, carries out any initialization, and then broadcasts a complete copy of the results to the worker nodes. This is done only once. When the master mode reaches the field and dipole evaluation stage it broadcasts a copy of the coordinates of all the dipoles and atoms to all the nodes. The nodes (including the master) then execute a sub-set of the lattice calculations in parallel. After this process is complete, all the partial forces are gathered from the nodes into the master node. The master node then performs the rest of the calculation serially and updates the information globally by broadcasting the new coordinates to all the worker nodes. The potential problem of load balancing has been overcome in the AMBER molecular dynamics software by a special load-balancing algorithm. The work is shared as evenly as possible initially and then readjusted at the force calculation stage to ensure that all the nodes have about the same workload.

References

[1] A. Grossfield, J. Sachs, T.B. Woolf. Dipole lattice membrane model for protein calculations. *Proteins*, **41**, 211–223 (2000).
[2] K. Makrodimitris, E.J. Fernandez, T.B. Woolf, J.P. O'Connell. Mesoscopic simulation of adsorption of peptides in a hydrophobic chromatography system. *Anal. Chem.*, (2004) (in press).
[3] P. Langevin. Une formule fondamentale de theorie cinetique. *Anal. Chem.*, **5**, 245–288 (1905).
[4] P. Debye. *Polar Molecules*, Vol., 1st ed., The Chemical Catalog Company, New York (1929).
[5] A. Warshel, S.T. Russell. Calculations of Electrostatic Interactions in Biological Systems and in Solutions. *Q. Rev. Biophys.*, **17**, 283–422 (1984).
[6] S.H. White, W.C. Wimley. Membrane protein folding and stability: physical principles. *Ann. Rev. Biophys. Biomol. Struc.*, **28**, 319–365 (1999).

[7] T.B. Woolf, B. Roux. Molecular dynamics simulation of the gramicidin channel in a phospholipid bilayer. *Proc. Natl Acad. Sci. USA*, **91**, 11631–11635 (1994).
[8] T.B. Woolf, B. Roux. Structure, energetics, and dynamics of lipid-protein interactions: A molecular dynamics study of the gramicidin A channel in a DMPC bilayer. *Proteins*, **24**, 92–114 (1996).
[9] M.T.W. Hearn. Reversed phase and hydrophobic chromatography of peptides and proteins. In *HPLC of Biological Macromolecules: Methods and Applications*, K.M. Gooding, F.E. Regnier (Eds.), pp. 99–245, Marcel Dekker Inc, New York (2001).
[10] K. Biswas, D. DeVido, J. Dorsey. Evaluation of methods for measuring amino acid hydrophobicities and interactions. *J. Chromatogr. A*, **1000**, 637–655 (2003).
[11] S. Klatte, T. Beck. Microscopic simulation of solute transfer in reversed phase liquid chromatography. *J. Phys. Chem.*, **100**, 5931–5934 (1996).
[12] C. Roth, A. Lenhoff. Electrostatic and van-der-Waals contributions to protein adsorption—comparison of theory and experiment. *Langmuir*, **11**, 3500–3509 (1995).
[13] J. Slusher, R. Mountain. A molecular dynamics study of a reversed-phase liquid chromatography model. *J. Phys. Chem. B*, **103**, 1354–1362 (1999).
[14] I. Yarovsky, M.L. Aguilar, T.W. Hearn. Influence of the chain-length and surface-density on the conformation and mobility of N-alkyl ligands chemically immobilized onto a silica surface. *Anal. Chem.*, **67**, 2145–2153 (1995).
[15] I. Yarovsky, M. Hearn, M. Aguilar. Molecular simulation of peptide interactions with an RP-HPLC sorbent. *J. Phys. Chem. B*, **101**, 10962–10970 (1997).
[16] J.L. Meek. Prediction of peptide retention times in high-pressure liquid chromatography on the basis of amino acid composition. *Proc. Natl Acad. Sci. USA*, **77**, 1632–1636 (1980).
[17] C. Horváth, M. Melander, I. Molnár. Solvophobic interactions in liquid chromatography with nonpolar stationary phases. *J. Chromatogr. A*, **125**, 129–156 (1976).
[18] B. Roettger, J. Myers, M. Ladisch, F. Regnier. Adsorption phenomena in hydrophobic interaction chromatography. *Biotechnol. Prog.*, **5**, 79–88 (1989).
[19] K. Dill. The mechanism of solute retention in reversed-phase liquid chromatography. *J. Phys. Chem.*, **91**, 1980–1988 (1987).
[20] C. Mazza, N. Sukumar, C. Breneman, S. Cramer. Prediction of protein retention in ion-exchange systems using molecular descriptors obtained from crystal structure. *Anal. Chem.*, **73**, 5457–5461 (2001).
[21] C.J.F. Böttcher. *Theory of Electric Polarization*, Vol., 2nd ed., Elsevier, Amsterdam (1973).
[22] W.D. Cornell, P. Cieplak, C.I. Bayly, I.R. Gould, K.M. Merz, D.M. Ferguson, D.C. Spellmeyer, T. Fox, J.W. Caldwell, P.A. Kollman. AMBER. *J. Am. Chem. Soc.*, **117**, 5179–5197 (1995).
[23] B.R. Brooks, R.E. Bruccoleri, B.D. Olafson, D.J. States, S. Swaminathan, M.J. Karplus. CHARMM—A program for macromolecular energy, minimization and dynamics calculations. *J. Comput. Chem.*, **4**, 187–217 (1983).
[24] T. Halgren. Merck molecular force field.1. Basis, form, scope, parameterization, and performance of MMFF94. *J. Comput. Chem.*, **17**, 490–519 (1996).
[25] J. Israelachvili. *Intermolecular and Surface Forces*, Vol., 2nd ed., Academic Press, San Diego, CA (1991).
[26] A. Bondi. Van der Waals volumes and radii. *J. Phys. Chem.*, **68**, 441–450 (1964).
[27] V.A. Daragan, K.H. Mayo. Motional model analyses of protein and peptide dynamics using *13C* and NMR relaxation. *Prog. Nucl. Magn. Reson. Spectrosc.*, **31**, 63–105 (1997).
[28] N. Davidson. *Statistical Mechanics*, McGraw-Hill Book Company, Inc., New York (1962).
[29] K. Makrodimitris, E.J. Fernandez, T.B. Woolf, J.P. O'Connell. Modeling the temperature and cosolvent effects in a hydrophobic chromatography system. *Biotechnol. Prog.* (in press).
[30] J. Cogswell. *C++ All-In-One Desk Reference For Dummies*, Vol. 2, 1st ed., Wiley Publishing Inc., Indianapolis, IN (2003).
[31] F. Booth. The dielectric constant of water and the saturation effect. *J. Chem. Phys.*, **19**, 391–394 1327, 1615 (1951).
[32] www.chemcomp.com, *Molecular Operating Environment*, Chemical Computing Group Inc, Montreal, Canada (2003).
[33] K. Hinsen. *The Molecular Modeling Toolkit: A Case Study of a Large Scientific Application in Python in Proceedings of the 6th International Python Conference*, CNRI, CA, USA (1997).
[34] W. Gropp, S. Huss-Lederman, A. Lumsdaine, E. Lusk, B. Nitzberg, W. Saphir, M. Snir. *MPI -THE COMPLETE REFERENCE Volume 2. The MPI Extensions*, Vol. 1, 2nd ed., The MIT Press, Cambridge, MA (1998).
[35] M. Snir, S. Otto, S. Huss-Lederman, D. Walker, J. Dongarra. *MPI - THE COMPLETE REFERENCE Volume 1. The MPI Core*, Vol., ed., The MIT Press, Cambridge, MA (1998).
[36] W. Smith. Molecular dynamics on hypercube parallel computers. *Comput. Phys. Commun.*, **62**, 229–248.
[37] L. Kale, R. Skeel, M. Bhandarkar, R. Brunner, A. Gursoy, N. Krawetz, J. Phillips, A. Shinozaki, K. Varadarajan, K. Schulten. NAMD2: Greater scalability for parallel molecular dynamics. *J. Comput. Phys.*, **151**, 283–312 (1999).
[38] J.M. Sokol, B.H. Holmes, J.P. O'Connell, E.J. Fernandez. Aprotinin conformational distributions during reversed-phase liquid chromatography. Analysis by hydrogen-exchange mass spectrometry. *J. Chromatogr. A*, **1007**, 55–66 (2003).
[39] K. Makrodimitris, G. Papadopoulos, C. Philippopoulos, D. Theodorou. Parallel tempering method for reconstructing isotropic and anisotropic porous media. *J. Chem. Phys.*, **117**, 5876–5884 (2002).
[40] J. Florián, A. Warshel. Langevin dipoles model for *ab initio* calculations of chemical processes in solution: parameterization and application to hydration free energies of neutral and ionic solutes and conformational analysis in aqueous solution. *J. Phys. Chem. B*, **101**, 5583–5595 (1997).
[41] K. Makrodimitris, E.J. Fernandez, T.B. Woolf, J.P. O'Connell. Simulations of peptides in reversed phase chromatography with a combination of adsorptive langevin lattice dipole method and nernst poisson boltzmann law. *(In preparation)*, (2005).
[42] K.A. Sharp. Polyelectrolyte electrostatics-salt dependence, entropic, and enthalpic contributions to free-energy in the nonlinear Poisson-Boltzmann model. *Biopolymers*, **36**, 227–243 (1995).
[43] C. Whitehead, C. Breneman, N. Sukumar, M. Ryan. Transferable atom equivalent multicentered multipole expansion method. *J. Comput. Chem.*, **24**, 512–529 (2003).